RESEARCH ARTICLE

STRUCTURAL BIOLOGY

A human postcatalytic spliceosome structure reveals essential roles of metazoan factors for exon ligation

Sebastian M. Fica*, Chris Oubridge, Max E. Wilkinson, Andrew J. Newman, Kiyoshi Nagai*

During exon ligation, the *Saccharomyces cerevisiae* spliceosome recognizes the 3′-splice site (3′SS) of precursor messenger RNA (pre-mRNA) through non–Watson-Crick pairing with the 5′SS and the branch adenosine, in a conformation stabilized by Prp18 and Prp8. Here we present the 3.3-angstrom cryo–electron microscopy structure of a human postcatalytic spliceosome just after exon ligation. The 3′SS docks at the active site through conserved RNA interactions in the absence of Prp18. Unexpectedly, the metazoan-specific FAM32A directly bridges the 5′-exon and intron 3′SS of pre-mRNA and promotes exon ligation, as shown by functional assays. CACTIN, SDE2, and NKAP—factors implicated in alternative splicing—further stabilize the catalytic conformation of the spliceosome during exon ligation. Together these four proteins act as exon ligation factors. Our study reveals how the human spliceosome has co-opted additional proteins to modulate a conserved RNA-based mechanism for 3′SS selection and to potentially fine-tune alternative splicing at the exon ligation stage.

T he spliceosome excises introns from precursor messenger RNAs (pre-mRNAs) to produce mature mRNA in two sequential transesterifications—branching and exon ligation—catalyzed at a single active site (1–3). The spliceosome assembles de novo on each pre-mRNA from component small nuclear ribonucleoproteins (snRNPs) and undergoes numerous conformational changes mediated by trans-acting proteins and DEAx/H-box adenosine triphosphatases (ATPases) (4). A series of cryo–electron microscopy (cryo-EM) structures of *Saccharomyces cerevisiae* (hereafter referred to as yeast) spliceosomes at different stages of assembly, catalysis, and disassembly have rationalized decades of biochemical and genetic data and have provided considerable mechanistic insights into how the spliceosome achieves these two trans-esterification reactions (1, 5–9). During initial assembly, the U1 snRNP base-pairs with the 5′-splice site (5′SS), whereas the U2 snRNP forms the branch helix through pairing around the branch point (BP) adenosine. Prespliceosome formation, involving minimal interaction between the U1 and U2 snRNPs in yeast, brings the 5′SS and the BP sequence into one assembly. In mammals, formation of the prespliceosome is promoted and regulated by many alternative splicing factors (10, 11). The prespliceosome then associates with the U4/U6-U5 tri-snRNP to form the pre-B com-plex, which is converted via B to B^{act} when U1 and U4 snRNPs dissociate by the activities of Prp28 and Brr2, which is followed by binding of the multisubunit Prp19-associated (NTC) and Prp19-related (NTR) complexes. The 5′SS is handed off to the U6 small nuclear RNA (snRNA), and the catalytic core is formed during this conversion. The catalytic core of the spliceosome comprises U6 and U2 snRNAs folded into a compact structure that binds two catalytic divalent ions (12–14). The 5′SS is positioned precisely at the catalytic metal ions by pairing between the conserved 5′-intron sequence, GUAUGU, and the ACAGAGA sequence of U6 snRNA and between the 5′-exon and U5 snRNA loop I (15, 16). During Prp2-induced remodeling to B*, the branch helix is docked into the active site by the branching factors Cwc25 and Yju2, which allows the 2′-hydroxyl group of the BP adenosine to attack the 5′SS, producing the free 5′-exon and a lariat intron–3′exon intermediate (1). Prp16-induced dissociation of the branching factors from the resulting C complex promotes rotation of the branch helix out of the active site (17). Exon ligation factors lock the branch helix into its new position in the resulting C* complex (5, 6). The 3′SS is positioned at the catalytic metal ions by non–Watson-Crick base-pairing between the last intron nucleotide G and the first intron nucleotide G, as well as between the penultimate intron nucleotide A and the BP adenosine. This configuration allows the 3′-hydroxyl group of the 5′-exon to attack the 3′SS, ligating the 5′- and 3′-exons into mRNA (7–9). The DEAH-box ATPase Prp22 then releases the resulting mRNA from the postcatalytic P complex (18, 19), and finally the ATPase Prp43 disassembles the spliceosome for new rounds of splicing (1–3).

Human spliceosomes are larger than their yeast counterparts and contain many additional proteins (3, 20, 21). Cryo-EM structures of the human spliceosomes captured at near-atomic resolution in different states confirm that the general architecture of the spliceosome is largely conserved between yeast and humans and reveal how some additional human proteins are integrated into the conserved architecture of the spliceosome (22–27). However, the functions of these proteins have not been determined experimentally. It is also not known if these proteins are constitutive components of the human spliceosome or whether some of them regulate alternative splicing of subsets of pre-mRNAs in a tissue-specific manner. Here we report the cryo-EM structure of the human postcatalytic spliceosome, which shows that the 3′SS is recognized through RNA-RNA interactions conserved between humans and yeast. Our high-resolution structure reveals that four proteins, not previously observed in human spliceosome structures, stabilize the branch helix and the docked 3′SS to facilitate exon ligation.

Purification and overall structure of the human P complex

The P-complex spliceosome was assembled on MINX pre-mRNA in HeLa nuclear extract supplemented with recombinant hPrp22 (DHX8) mutant (K594A; see supplementary note 1 and fig. S1) to prevent release of ligated exons. Oligonucleotide-directed RNase H digestion was targeted to the region of the 3′-exon protected only when the 3′SS is docked into the active site. The resulting P complex was affinity-purified on amylose-resin by using three MS2 aptamers attached to the 3′-exon to eliminate contaminating C* complex (supplementary methods; figs. S1 and S2) (7).

The overall architecture of the human P complex obtained by cryo-EM reconstruction at 3.3 Å resolution (supplementary materials PyMOL session, figs. S2 to S5) is similar to that of the human C* complex determined at an average resolution of 3.76 Å (22) and 5.9 Å (26) (Fig. 1). The higher resolution of our cryo-EM density map of the human P complex allowed us to build more-complete models of proteins in the peripheral region (table S2) and parts of four additional proteins (Cactin, FAM32A, SDE2, and NKAP) not present in *S. cerevisiae* (Fig. 1, B and C, and figs. S5 and S6). The remaining parts of these proteins are predicted to be largely disordered. The densities for Cactin and FAM32A were partially visible in the map of the C* complex (22) but were not of sufficient quality for model building. The higher-resolution map of our P complex allowed us to build the C-terminal half of FAM32A based on density alone, but the highly charged N-terminal half is disordered (fig. S6).

A conserved 3′SS recognition mechanism

The RNA-based active site of the human P complex is essentially unchanged compared to C*,

with the U2 and U6 snRNAs forming a triple helix that binds two catalytic Mg^{2+} ions (fig. S7). In the human P complex, the newly formed mRNA remains bound at the active site through its 5′-exon pairing to U5 snRNA (fig. S7A). The new phosphodiester bond connecting the 5′-exon to the first two nucleotides of the 3′-exon is clearly visible, confirming that our sample represents the genuine P complex (fig. S5B). Clear density

extending from the intron G(+1) and the BP adenosine could be modeled as the last three nucleotides of the 3′SS (Fig. 1E and fig. S5B). As in yeast, the Hoogsteen edge of the 3′SS G(−1) forms a base pair with the Watson-Crick edge of the 5′SS G(+1). Additionally, N7 of the 3′SS A (−2) forms an H-bond with N6 of the BP adenosine. Thus, the 3′SS is recognized, as in yeast (Fig. 1, E and F), through pairing with the 5′SS and the

BP adenosine. The 5′SS U(+2) pairs with the U6 snRNA A51, which stacks on the 3′SS G(−1), an interaction that was not modeled in the human C* complex (22) and which allows the 3′-hydroxyl of 3′SS G(-1) to project into the active site. Docking

Fig. 1. Structure of a human P complex reveals unexpected exon ligation factors.
(A) Overview of the human P complex spliceosome complex. EJC, exon junction complex; NTC, Prp19-associated complex; NTR, Prp19-related complex. (B and C) Comparison of the P (present work) and C* (22) complexes reveals previously unknown factors. The presence of mRNA and the docked 3′-splice site in our P-complex structure are apparent. Dashed lines indicate possible path of the intron not visible in the density. The intron is shown in gray, the 5′-exon in orange, and the 3′-exon in yellow. Prp8^{EN}, Prp8 endonuclease domain; Prp8^{N}, Prp8 N-terminal domain. (D) Binding of the substrate in the active site cavity of P complex. Prp8^{RT}, Prp8 reverse-transcriptase domain. (E) The 3′SS is recognized by the 5′SS and the BP adenosine in the human P complex. (F) 3′SS recognition in the yeast P complex (7).

Fig. 2. FAM32A is a component of the P-complex active site. (A and B) FAM32A binds Prp8 and projects its C terminus into the RNA catalytic core. Prp8^{RH}, Prp8 RNase H domain, Prp8^{N}, N-terminal domain of Prp8. (C) FAM32A stabilizes the 5′-exon onto U5 snRNA loop I, in proximity to the docked 3′SS. The highly conserved FAM32A C terminus across metazoans is apparent; variable residues are shaded gray. Dashed lines indicate possible path of the intron not visible in the density. Single-letter abbreviations for the amino acid residues are as follows: A, Ala; D, Asp; E, Glu; F, Phe; H, His; I, Ile; K, Lys; L, Leu; M, Met; N, Asn; P, Pro; Q, Gln; R, Arg; S, Ser; T, Thr; V, Val; W, Trp; and Y, Tyr.

of the 3'SS onto the 5'SS is stabilized by the Prp8 alpha-finger and beta-finger—another feature similar to that of yeast (Fig. 1D). However, Prp18—which in yeast projects into the active site and stabilizes the intron upstream of the 3'SS at positions –3 to –5—was not observed in our map and was not detected by mass spectrometry either in our sample or in previous mass-spectrometric studies of C* and P complexes (20, 26, 27). Indeed, beyond the 3'SS C(–3), the intron becomes disordered in our map. The remaining nucleotides between the 3'SS and the branch helix loop out of the spliceosome, and their path is likely guided by mammalian-specific proteins, as described below.

FAM32A is a metazoan-specific exon ligation factor

The most notable finding in our structure is that FAM32A (figs. S5C and S6), a poorly characterized protein of 13 kDa, binds between the endonuclease (EN) and N-terminal (N) domains of Prp8 and projects its C terminus deep into the active site (Fig. 2, A and B). Here FAM32A stabilizes the pairing between the 5'SS, the 3'SS,

and the BP adenosine together with the alpha-finger and beta-finger of Prp8 (Fig. 2A). The C terminus of FAM32A binds along the 5'-exon through direct contacts between K107 and S109 and the phosphates of C(–2) and G(–1), respectively, and stabilizes its base-pairing to loop I of U5 snRNA (Fig. 2C). The positively charged side chain of its C-terminal K112 extends into the space where the 5'SS, 3'SS, and BP come together to promote docking of the 3'SS (Fig. 2C). FAM32A is also known as ovarian tumor associated gene–12 (OTAG-12) and is down-regulated in a mouse model of ovarian tumor development (28). The OTAG-12 gene is expressed as three splice isoforms—OTAG-12a, OTAG-12b, and OTAG-12c—in mice (figs. S5C and S6 and supplementary note 2), and expression of the full-length OTAG-12b in ovarian cancer and human embryonic kidney 293 (HEK293) cells suppressed cell growth whereas OTAG-12c with N-terminal deletion or OTAG-12a with altered C-terminal sequence had no such effect. FAM32A (OTAG-12b, fig. S6B) bound in the P complex promotes mRNA formation for proapoptotic genes, acting as a tumor suppressor. Indeed, the entire C terminus of FAM32A is es-

sentially invariant in metazoans from zebrafish to humans (Fig. 2C), consistent with a role in regulating splicing.

Depletion of FAM32A from HeLa nuclear extracts impaired exon ligation (Fig. 3, A to E, and fig. S8, A to C), causing accumulation of cleaved 5'-exon at the C* stage (fig. S8, D and E). Recombinant FAM32A restored efficient mRNA formation (Fig. 3D and fig. S8, B and C), demonstrating that FAM32A promotes splicing by facilitating exon ligation, in agreement with our structure. Ultraviolet (UV) cross-linking using pre-mRNA containing a single 4-thioU substitution at position –2 of the 5'-exon (Fig. 3, C, D, F, and G) produced two major cross-links (Fig. 3, F and G). The one above 200 kDa represents Prp8, whereas the cross-link between 15 and 25 kDa was confirmed to be FAM32A by depletion and addition of slightly larger, tagged FAM32A (Fig. 3, G and H). P complexes assembled in FAM32A-depleted extracts contained mostly lariat-intermediate and cleaved 5'-exon, which cross-linked to residual FAM32A, demonstrating that FAM32A also binds the 5'-exon in the precatalytic C* complex (Fig. 3, F and G). Thus, FAM32A is a bona fide exon ligation factor that stabilizes docking of the 3' SS into the active site and promotes splicing in mammals.

NKAP and FAM32A stabilize Slu7 binding

As in yeast, Slu7 rigidifies the C*/P conformation by binding across the Prp8 EN and N domains (Fig. 1C and 4, A to C). Binding of the central region of Slu7 to the Prp8 EN domain is stabilized by FAM32A (Fig. 2B), whereas nuclear factor κB–activating protein (NKAP)—a previously unidentified factor—promotes binding of the Slu7 N terminus onto Prp8 (Fig. 4C and fig. S5D). NKAP is a 415-residue protein implicated in T cell development; it consists of highly charged repetitive sequences such as Ser-Arg and poly-Lys and is expected to be intrinsically disordered through almost its entire length. However, residues 329 to 358 form a short helix that bridges the N- and C-terminal fragments of Slu7 bound to Prp8 and stabilizes the P complex. Indeed, NKAP binds exon sequences genome-wide and associates with mRNA in vitro, and depletion of NKAP in vivo reduces splicing efficiency, consistent with a role in promoting mRNA formation (29).

Cactin, SDE2, and PRKRIP1 stabilize the branch helix

The branch helix is locked into position by the WD40 domain of Prp17, CDC5L (Cef1), and CRNKL1 (Clf1), as in yeast C* and P complexes (5, 7–9) (Fig. 4, D to G). Unexpectedly, the human P complex structure revealed that the branch helix is further secured in its exon ligation conformation by Cactin, SDE2, and PRKRIP1. Our cryo-EM map enabled us to build residues between 637 and 756 of Cactin, which folds into a β-sandwich domain. Its N-terminal region has long stretches of charged and polar amino acids, suggesting that these regions are intrinsically disordered. Its C terminus and a short α helix protruding from the
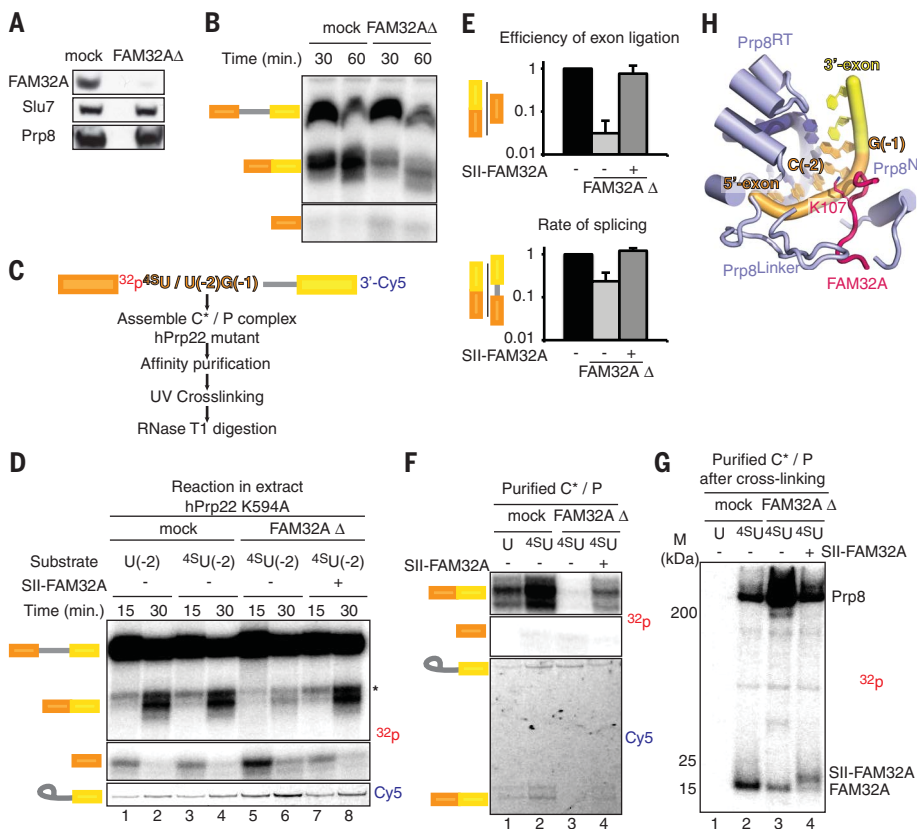

Fig. 3. FAM32A promotes exon ligation by binding the 5'-exon. (A and **B)** Depletion of FAM32A impairs exon ligation. (**C)** Overview of the UV cross-linking experiment. C(−2) was changed to U(−2) for these experiments. (**D)** FAM32A promotes exon ligation. (**E)** Effect of FAM32A depletion on exon ligation efficiency. Experiments were performed using a substrate with a single ^{32}P at U(−2) of the 5'-exon. Error bars represent SD (n = 3). (**F)** C* complexes accumulate in FAM32A-depleted extracts. Shown is RNA extracted from affinity-purified P complexes (see also fig. S8). (**G)** FAM32A cross-links to the 5'-exon. SDS–polyacrylamide gel electrophoresis of proteins labeled through cross-linking. SII-FAM32A, Strep-tactin–tagged FAM32A; ^{32}p, ^{32}P radioactive phosphate; ^{4S}U, 4-thio-uridine. (**H)** Positioning of FAM32A and Prp8 around C(−2) of the 5'-exon rationalizes the cross-linking results.

β-sandwich domain interact with the Prp8 RNase H domain (Fig. 4, D and E), allowing Cactin to project a series of charged residues toward the branch helix, near the predicted path of the intron between the BP and the docked 3′SS (Fig. 4E), stabilizing 3′SS docking. Finally, a loop just before the C-terminal β strand of Cactin forms an extensive positively charged surface with the N-terminal region of CRNKL1 and with Cdc5L that surrounds the branch helix (Fig. 4, F and G). This surface is stabilized by an α helix of SDE2 that interacts with CRNKL1 and Cdc5L (Fig. 4G and fig. S9A). Our map also enabled us to build 30 additional residues of PRKRIP1 (*22*), which reveals its distinctive structure (fig. S9, B and C). The N-terminal residues 28 to 39 form an α helix that bridges between the U2 Sm ring and U2 snRNA at the tip of the branch helix. Together with the long C-terminal α helix bound to stem IV of U2 snRNA, it locks the branch helix into the exon-ligation orientation (fig. S9B). The intervening loop inserts into the active site and interacts with the Prp8 RNase H domain and the C terminus of Cactin to stabilize the branch helix and promote exon ligation.

SDE2 is first synthesized as an inactive precursor containing an N-terminal ubiquitin-fold domain, which is cleaved to produce activated Sde2-C. Our structure shows that the N-terminal ubiquitin domain of unprocessed SDE2 would clash with the branch helix (Fig. 4, F and G), explaining why the full-length protein cannot be incorporated into the spliceosome, as shown in *Schizosaccharomyces pombe*. *S. pombe* cells that cannot produce Sde2-C show defects in splicing of the same specific introns as cells lacking Cactin (*30*), suggesting that binding of Cactin and Sde2 to the spliceosome is highly cooperative. Indeed, cells lacking Sde2-C show reduced Cactin binding to the spliceosome (*30*). The P-complex structure shows how SDE2 guides CRNKL1 to bind Cactin (Fig. 4G), thus rationalizing the functional observations in *S. pombe*.

Discussion

The human P-complex structure shows that the 3′SS is recognized and docked into the active site of the spliceosome on the basis of the same base-pairing interactions seen in the yeast P complex (*7–9*). Similarly to yeast, a set of conserved factors including the RNase H domain of Prp8, Prp17, and Slu7 rigidify the position of the branch helix in the P complex and promote 3′SS docking (*7*). Unexpectedly, our high-resolution map of human P complex enabled us to build four additional proteins—FAM32A, Cactin, SDE2, and NKAP, which have been identified by mass spectrometry but have not been found in any of the cryo-EM structures of human spliceosomes (*22–26*). Three of these factors—NKAP, Cactin, and Sde2—cooperate with PRKRIP1 to lock the branch helix in place in P complex (Fig. 5). Indeed, Cactin and Sde2 promote splicing of the same specific subset of introns in *S. pombe* (*31*), highlighting their role in exon ligation, although the basis of their specificity is not understood. Together these factors partially compensate for the absence of Yju2, which
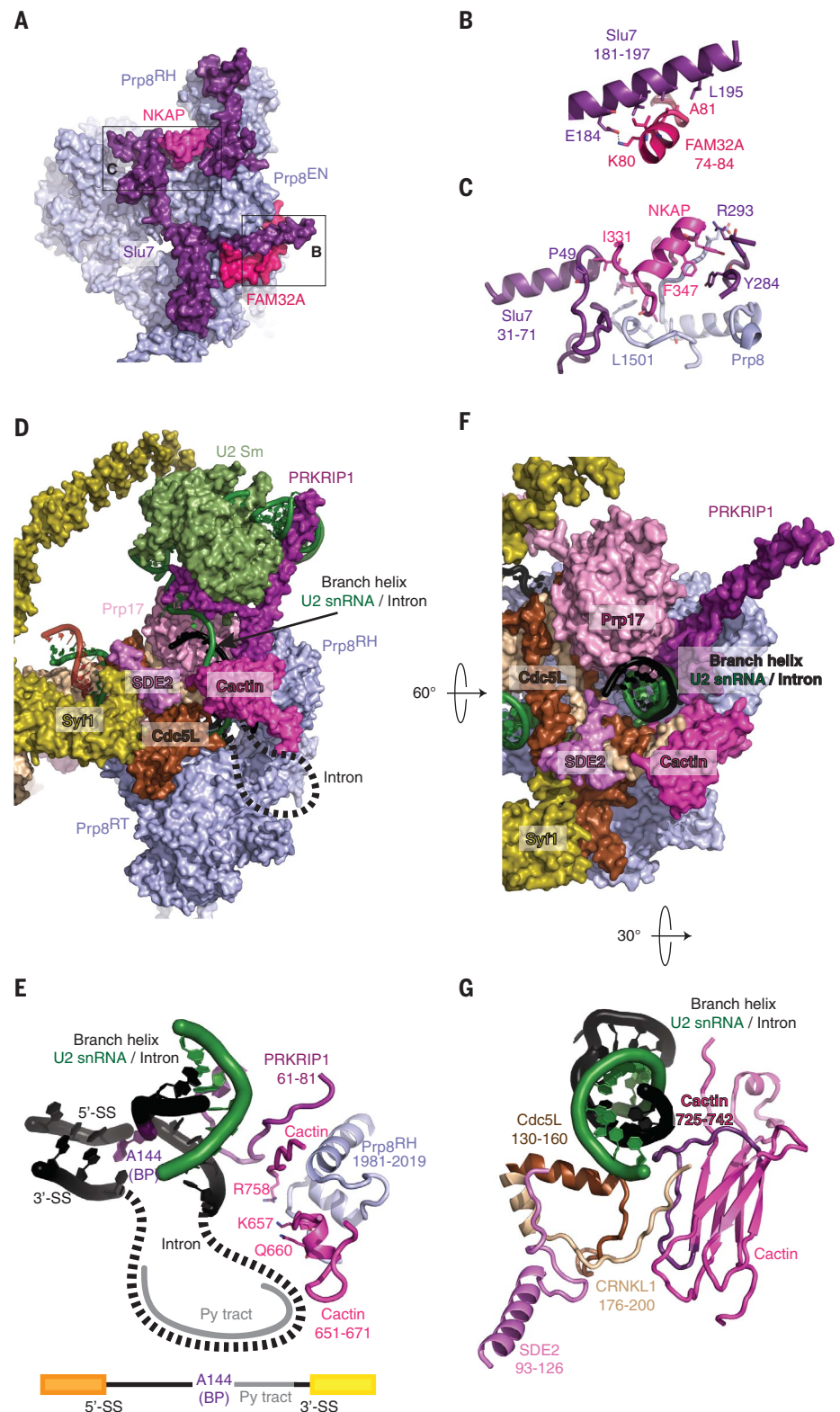
Fig. 4. Unexpected factors stabilize the P-complex conformation. (**A** to **C**) FAM32A and NKAP promote binding of Slu7 to the P complex. Prp8EN, Prp8 endonuclease domain. (**D** and **E**) Cactin stabilizes the position of the branch helix for exon ligation. Dashed lines indicate possible path of the intron not visible in the density. Py tract, polypyrimidine tract. (**F**) Previously unidentified factors position the branch helix. (**G**) SDE2 promotes Cactin binding near the branch helix. The loop of Cactin that projects a positive surface onto the branch helix is highlighted in magenta.
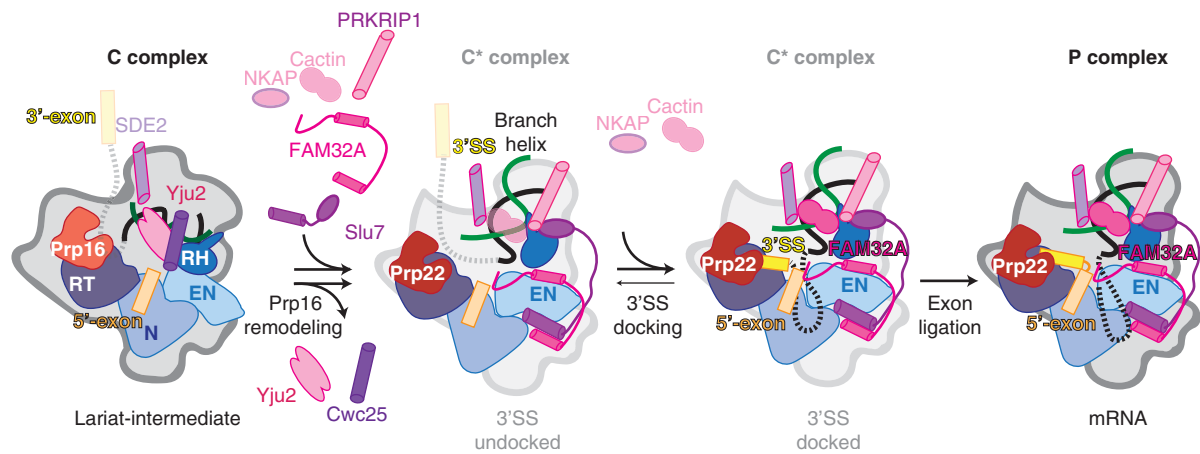
Fig. 5. Model for the action of exon ligation factors in metazoans. After Prp16 dissociates Cwc25 and Yju2 from C complex, Slu7, PRKRIP1, and FAM32A can bind the remodeled C* conformation. Cactin may bind before, or concomitantly with, docking of the 3′-exon at the catalytic core and associates more strongly upon 3′SS docking. SDE2 is likely present already in the C complex, as it interacts with the NTC, remains bound throughout the catalytic stage, and promotes Cactin binding after remodeling by Prp16. FAM32A binds the 5′-exon and likely stabilizes docking of the 3′SS onto the 5′SS and BP adenosine.

stabilizes the branch helix in the yeast P complex (fig. S10B) but which dissociates during the C to C* transition in humans (Fig. 5) (7).

In yeast, docking of the 3′SS is stabilized by Prp18, which abuts the 3′SS and guides Slu7 binding to Prp8. Indeed, in a subset of the yeast P-complex particles lacking Prp18 and Slu7 (7), the 3′SS is not stably docked in the active site and the branch helix shows weaker density, suggesting that the branch helix is mobile (7). By contrast, Prp18 was not detected by mass spectrometric analysis of the human C* and P complex spliceosome assembled on MINX pre-mRNAs (20, 26, 27), and Prp18 is absent in the cryo-EM structure of the human C* complex (22). The human P-complex structure presented here also lacks Prp18 (fig. S10, A and B, and table S3).

Notably, FAM32A penetrates into the active site of the P-complex spliceosome assembled on MINX pre-mRNA and promotes 3′SS docking, thus partly substituting for Prp18. In contrast, depletion of Prp18 from HeLa extracts abolishes exon ligation of β-globin pre-mRNA (32), raising the intriguing possibility that Prp18 promotes splicing of a subset of human transcripts, acting as in yeast. Indeed, in *S. pombe*, genetic depletion of Prp18 abolishes splicing in an intron-specific manner (33). Docking of the yeast Prp18 structure onto our human P complex indicates that Prp18 binding can be accommodated while FAM32A is bound in the active site of the human P complex (fig. S10, C and D). Hence, both Prp18 and FAM32A could influence alternative splicing of specific pre-mRNAs at the exon ligation stage. Consistent with this idea, Slu7 has been shown to influence selection of competing 3′SS by regulating docking of the 3′SS at the P-complex stage (34). Intriguingly, Slu7 does not closely approach the active site in our human P complex but binds FAM32A, which enters the active site. Thus, FAM32A could be responsible, at least in part, for the effects of Slu7 on 3′SS selection. Therefore, several exon ligation factors could modulate 3′SS choice during the catalytic stage.

Our P-complex structure highlights how in mammals specific proteins regulate a conserved mechanism for 3′SS recognition, and it also provides a framework to expand mechanistic studies of the human spliceosome to different cell types and different metabolic or developmental states.

REFERENCES AND NOTES

1. C. Plaschka, A. J. Newman, K. Nagai, *Cold Spring Harb. Perspect. Biol.* (2019).
2. C. Yan, R. Wan, Y. Shi, *Cold Spring Harb. Perspect. Biol.* **11**, a032409 (2019).
3. B. Kastner, C. L. Will, H. Stark, R. Lührmann, *Cold Spring Harb. Perspect. Biol.* (2019).
4. O. Cordin, J. D. Beggs, *RNA Biol.* **10**, 83–95 (2013).
5. S. M. Fica et al., *Nature* **542**, 377–380 (2017).
6. C. Yan, R. Wan, R. Bai, G. Huang, Y. Shi, *Science* **355**, 149–155 (2017).
7. M. E. Wilkinson et al., *Science* **358**, 1283–1288 (2017).
8. S. Liu et al., *Science* **358**, 1278–1283 (2017).
9. R. Bai, C. Yan, R. Wan, J. Lei, Y. Shi, *Cell* **171**, 1589–1598.e8 (2017).
10. Q. Pan, O. Shai, L. J. Lee, B. J. Frey, B. J. Blencowe, *Nat. Genet.* **40**, 1413–1415 (2008).
11. C. W. Smith, J. Valcárcel, *Trends Biochem. Sci.* **25**, 381–388 (2000).
12. T. A. Steitz, J. A. Steitz, *Proc. Natl. Acad. Sci. U.S.A.* **90**, 6498–6502 (1993).
13. S. M. Fica et al., *Nature* **503**, 229–234 (2013).
14. S. M. Fica, M. A. Mefford, J. A. Piccirilli, J. P. Staley, *Nat. Struct. Mol. Biol.* **21**, 464–471 (2014).
15. A. J. Newman, C. Norman, *Cell* **68**, 743–754 (1992).
16. E. J. Sontheimer, J. A. Steitz, *Science* **262**, 1989–1996 (1993).
17. D. R. Semlow, M. R. Blanco, N. G. Walter, J. P. Staley, *Cell* **164**, 985–998 (2016).
18. M. Company, J. Arenas, J. Abelson, *Nature* **349**, 487–493 (1991).
19. B. Schwer, *Mol. Cell* **30**, 743–754 (2008).
20. M. S. Jurica, L. J. Licklider, S. R. Gygi, N. Grigorieff, M. J. Moore, *RNA* **8**, 426–439 (2002).
21. S. Bessonov, M. Anokhina, C. L. Will, H. Urlaub, R. Lührmann, *Nature* **452**, 846–850 (2008).
22. X. Zhang et al., *Cell* **169**, 918–929.e14 (2017).
23. D. Haselbach et al., *Cell* **172**, 454–464.e11 (2018).
24. X. Zhang et al., *Cell Res.* **28**, 307–322 (2018).
25. X. Zhan, C. Yan, X. Zhang, J. Lei, Y. Shi, *Science* **359**, 537–545 (2018).
26. K. Bertram et al., *Nature* **542**, 318–323 (2017).
27. J. O. Ilagan, R. J. Chalkley, A. L. Burlingame, M. S. Jurica, *RNA* **19**, 400–412 (2013).
28. X. Chen, H. Zhang, J. P. Aravindakshan, W. H. Gotlieb, M. R. Sairam, *Oncogene* **30**, 2874–2887 (2011).
29. B. D. Burgute et al., *Nucleic Acids Res.* **42**, 3177–3193 (2014).
30. P. Thakran et al., *EMBO J.* **37**, 89–101 (2018).
31. L. E. Lorenzi et al., *EMBO J.* **34**, 115–129 (2015).
32. D. S. Horowitz, A. R. Krainer, *Genes Dev.* **11**, 139–151 (1997).
33. N. Vijaykrishna et al., *J. Biol. Chem.* **291**, 27387–27402 (2016).
34. K. Chua, R. Reed, *Nature* **402**, 207–210 (1999).

SUPPLEMENTARY MATERIALS

www.sciencemag.org/content/363/6428/710/suppl/DC1
Materials and Methods
Supplementary Text
Figs. S1 to S10
Tables S1 to S3
References (35–51)
PyMOL session

4 January 2019; accepted 21 January 2019
Published online 31 January 2019
10.1126/science.aaw5569

Science

A human postcatalytic spliceosome structure reveals essential roles of metazoan factors for exon ligation

Sebastian M. Fica, Chris Oubridge, Max E. Wilkinson, Andrew J. Newman and Kiyoshi Nagai

A human P spliceosome structure

Splicing of some pre–messenger RNAs could be regulated by cell type–specific splicing factors. Fica *et al.* describe the cryo–electron microscopy structure of the human postcatalytic (P) spliceosome. Surprisingly, it lacks the splicing factor Prp18, which plays an essential role in exon ligation in the yeast spliceosome. Instead, a metazoan-specific splicing factor, FAM32A, compensates for Prp18 and promotes exon ligation by penetrating the active sites and directly stapling the 5′ exon and the 3′ splice site. These findings suggest a way to control tissue-specific alternative splicing.

Science, this issue p. 710

ARTICLE TOOLS	http://science.sciencemag.org/content/363/6428/710
SUPPLEMENTARY MATERIALS	http://science.sciencemag.org/content/suppl/2019/01/30/science.aaw5569.DC1
REFERENCES	This article cites 51 articles, 14 of which you can access for free http://science.sciencemag.org/content/363/6428/710#BIBL
PERMISSIONS	http://www.sciencemag.org/help/reprints-and-permissions

Use of this article is subject to the Terms of Service